Pre-nucleation cluster formation upon ethyl acetate addition to an aqueous solution of an anionic hydrotrope

Asmae El Maangar, Pierre Degot, Verena Huber, Jérémy Causse, Patrick Berthault, Didier Touraud, Werner Kunz, Thomas Zemb

Version of Record: https://www.sciencedirect.com/science/article/pii/S0167732220311752
Manuscript_0672be9ec49504d1919033063768236e

Pre-nucleation cluster formation upon ethyl acetate addition to an aqueous solution of an anionic hydrotrope

Asmae El Maangar[a,*], Pierre Degot[b], Verena Huber[b], Jeremy Causse[a], Patrick Berthault[c], Didier Touraud[b], Werner Kunz[b], Thomas Zemb[a]

[a]*ICSM, Univ Montpellier, CEA, CNRS, ENSCM, Marcoule, France*
[b]*Institute of Physical and Theoretical Chemistry, University of Regensburg, D-93040 Regensburg, Germany*
[c]*Université Paris-Saclay, CEA, CNRS, NIMBE, 91191, Gif-sur-Yvette, France*

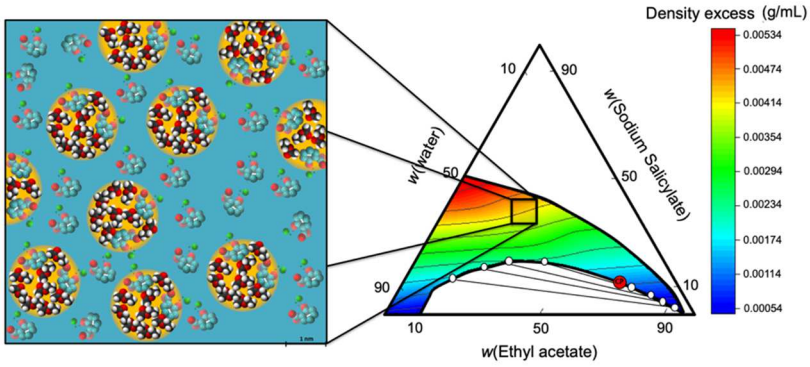

GRAPHICAL ABSTRACT

ABSTRACT

Hydrotropes are used to solubilise poorly soluble solutes. Here the general features of the solution behaviour of the very common anionic hydrotrope sodium salicylate is investigated. With the use of density and scattering measurements, it is demonstrated that around the critical point neither pre-Ouzo structuring nor an Ouzo effect are present. By contrast, in a domain near the liquid-solid phase boundary, X-ray light and neutron scattering combined with a density excess determination prove the presence of dynamic aggregates. These aggregates are stabilized without any surfactants, but by selective solvation of ethyl acetate, reminiscent of stable liquid pre-nucleation aggregates. And most surprising: in water saturated by ethyl acetate (20 % wt), sodium salicylate micellizes like a medium chain classical surfactant.

Keywords: hydrotrope; sodium salicylate; ethyl acetate; pre-nucleation aggregate; critical phase separation;

1. Introduction

To solubilize hydrophobic components in water, usually surfactants are used. An alternative is the use of a hydrotrope [1]. This is a component that is amphiphilic and highly soluble in water, but does not permit the formation of defined structures such as spherical micelles or liquid crystals. Instead, it may form ill-defined aggregates in water, but this is not mandatory. Often, hydrotropes only form such aggregates in the presence of a hydrophobic compound that the hydrotropes surround and, as a consequence, dissolve in an aqueous medium. There are different mechanisms through which hydrotropes enhance the solubility of a hydrophobic compound in water [2], but in all cases, the required hydrotrope concentrations are much higher (usually in the molar range) than the required surfactant concentrations to dissolve a significant amount of “oil”, meaning a hydrophobic component [3].

Surprisingly, such ternary, surfactant-free mixtures of water, hydrotrope and oil can even lead to long-time stable emulsions, as in the well-known Ouzo mixture [4]. In this case, essentially a homogeneous mixture of water,

* Corresponding author. Tel.: +33 466 79 77 18.
E-mail address: asmae.elmaangar@cea.fr (A. El Maangar)

ethanol (the hydrotrope) and anethol (the oil) can be diluted with water so that the phase unmix into two liquid phases. These phases do not separate immediately into two macroscopic liquid layers, but spontaneously form more or less very stable emulsions with very monodisperse drops, even in the absence of surfactants. This effect is termed the "Ouzo effect", and the driving forces for this phenomenon is still not fully understood.

However, there is another unusual phenomenon. For monophasic ternary mixtures of water, a hydrotrope and a hydrophobic compound such as the one in the original Ouzo mixture, more or less well-defined structures could be identified. These structures have been termed "pre-Ouzo structures" (and the corresponding, underlying effect the "pre-Ouzo effect") [5], since they were found at compositions close to the liquid-liquid phase boundary, where Ouzo emulsions spontaneously occur. These pre-Ouzo structures have a certain similarity to classical microemulsion systems, despite the fact that the hydrotropes are not surfactants. The structures can be swollen direct micelles, bicontinuous structures or reversed ones [6].

Since several years, there is a growing interest in the understanding of the Ouzo and pre-Ouzo effect, because they are widely used in industrial formulations and processes. However, until now, only ternary mixtures water-oil-hydrotrope with uncharged hydrotropes have been investigated [7], whereas for industrial applications, various types of charged hydrotropes are also widely used. A typical example is sodium cumene or xylene sulfonate in household cleansers.

In the present study, we consider another classical charged hydrotrope, namely sodium salicylate. This 1-1 electrolyte is widespread as a solubilizing agent (hydrotrope) in the pharmaceutical [8–16] and body care industry [17,18] to solubilize hydrophobic dyes, aroma, perfume or pharmaceutically active molecules in water. Especially for pharmaceutical applications, it is favorable to formulate stable colloidal solutions without classical surfactants.

Sodium salicylate has several advantages in formulation [1]. However, it is not fully miscible with ethyl acetate. On the other hand, due to its ionic character, it brings into the water-hydrotrope-oil system an additional interaction force, and we find it interesting to investigate, in how far this feature influences the structuring in the monophasic region of such a ternary mixture.

We consider here mixtures of water, sodium salicylate and a model oil, i.e., ethyl acetate, as a potentially powerful surfactant-free solubilisation system. Ethyl acetate (EA) is a green, bio-based solvent with a boiling point of 77 °C, a flash point of -4 °C and a partial vapor pressure of 10 kPa at room temperature. It is used in food industry as flavor (essence of fruit and synthetic flavor preparation) and as an efficient solvent for phenols [19,20]. EA is also used in the pharmaceutical industry as a non-toxic solvent [21]. We have shown recently that ethyl acetate/ethanol/water system is an efficient and a green broadband extracting mixture [22]. These findings made us investigate the macroscopic phase behaviour and the mesostructure present in the corresponding ternary phase diagram at room temperature. Here is now the extension to a similar system with a charged hydrotrope instead of ethanol.

2. Experimental

2.1. Materials

The synthetic phytochemical curcumin (> 97%) was bought from TCI (Eschborn, Germany). The solvents, 1-octanol (purity >99%), ethyl acetate (EA) (>99.9%), deuterated chloroform (CDCl3, >99.9%), acetone (≥ 99.9 %) and ethanol (≥ 99.9) were purchased from Merck (Darmstadt, Germany). Sodium salicylate (NaSal) (>99.5%), sodium dodecyl sulfate (SDS) (>98.5%), sodium xylene sulfonate (SXS) (>90%) and Disperse Red 13 (DR-13) (dye content 95%) were purchased from Sigma Aldrich (Darmstadt, Germany). Deuterated water (>99.96%) was purchased from Eurisotop (Saint-Aubin, France). All chemicals were used without further purification.

2.2. Disperse Red 13 solubilisation in the binary water/surfactant or hydrotrope systems

All solutions to be measured contained water and the hydrotrope or surfactant at different concentrations. The solutions were saturated with an excess of DR-13 and stirred for 24 hours at room temperature using a magnetic stirrer. The solutions were filtered subsequently in order to remove the excess of non-dissolved DR-13. Optical density measurements of the solutions were performed using a Lambda 18 UV/Vis spectrometer by Perkin Elmer (Waltham, USA). Suitable dilutions were made, when the measured optical density was above a critical value.

2.3. Ternary phase diagram determination

The determination of the existence of a clear, homogeneous, monophasic domain in the ternary water/sodium salicylate/ethyl acetate mixture was performed using a static and dynamic process, described by Clausse et.*al*. [23]. In screw tubes of borosilicate glass, sodium salicylate was mixed with ethyl acetate or water at determined weight fractions to obtain a starting weight of 3 g. Water or ethyl acetate, respectively, was added dropwise with Pasteur pipettes to the solutions, until a visible change in the phase behaviour occurred. Measurements were carried out at room temperature and the phase transitions were determined with the naked eye and through two cross-polarized filters in order to check the presence of liquid crystals.

The amount of water or ethyl acetate added until the phase transition occurred was obtained with precise weight measurements. The weight fractions were then calculated for each formulation and the pseudo-ternary phase diagram was built. The same method was used to obtain the phase diagram of water/ethanol/1-octanol and water/ethanol/EA.

2.4. Density measurements

Solution densities were determined using a vibrating tube density meter (DMA 5000 M, Anton Paar, Austria) at (25 ± 0.005) °C with a nominal precision of ± $5 \cdot 10^{-6}$ g/mL. Calibration was performed using air and pure water at 25 °C. At the beginning and at the end of each day, calibration was checked using pure water and between each measurement against air (maximum deviation: ± $5 \cdot 10^{-5}$ g/mL).

2.5. Tie-lines and critical point determination

In order to determine the position of the critical point in the system water/NaSal/EA, different ternary mixtures were prepared (each 4 g) within the clear and homogeneous region near the phase separation border, in closable, volume-scaled tubes of borosilicate glass at room temperature. A fixed small amount of water and EA was then added very slowly to reach the phase boundary. After complete phase separation, the volume ratio between water- and oil-rich phases was determined. The critical point corresponds to the extrapolation of the formulations, both having separated phases with equal volumes, to the phase boundary.

The end-points of the tie-lines were obtained through density measurements. Biphasic samples were prepared by mixing first the sodium salicylate and ethyl acetate. After addition of the residual amount of deuterium oxide, the solution was thoroughly mixed by hand. Subsequently, phase separation of the milky mixture was accelerated by gentle centrifugation (1500 g for 15 min) using a ROTINA 380 R centrifuge. The two phases obtained were carefully separated and collected in sealed vessels for density measurement. The determined densities were placed in the density map obtained before (see Figure 3 and supplementary material) to deduce the composition of both water-rich and oil-rich separated phases.

The same methods were used to obtain the critical point and the tie-lines of water/ethanol/1-octanol and water/ethanol/EA.

2.6. Dynamic light scattering

Dynamic light scattering (DLS) measurements were conducted using a temperature-controlled CGS-3 goniometer system by ALS (Langen, Germany), equipped with an ALV-7004/FAST Multiple Tau digital correlator and a vertically polarized 22 mW HeNe Laser (λ = 632.8 nm). The samples were filtered into dust-free cylindrical light-scattering cells (10 mm outer diameter) through 0.2 µm PTFE syringe filters before measuring. The sealed measuring cells were successively placed inside the apparatus. The measurements were performed at 25 ± 0.1 °C at a 90° scattering angle for 200 s.

2.7. X-ray scattering

Small- and Wide-Angle X-Ray Scattering experiments were carried out on the home-built SAXS camera at ICSM, using a bench built by Xenocs and x-ray radiation generated by a sealed molybdenum tube (wavelength λ = 0.71 Å). The large on-line detector (MAR Research 345, diameter = 345 mm) was located at 750 mm from the sample stage. Off-center detection was used to cover small and wide angles simultaneously. The two-dimensional spectra were integrated with the software FIT2D. Data were normalized taking into account the electronic background of the detector, transmission measurements, and empty cell subtraction. The acquisition time was 3600 s per sample.

2.8. Neutron Scattering

Small-angle neutron scattering measurements were performed at the French neutron facility Laboratoire Léon Brillouin/Orphée (LLB/Orphée, Saclay) on the PAXY spectrometer. The neutron wavelength was fixed at 4 Å using a monochromator. A 2D gas-filled detector settled at 1 m from the sample position, which allows covering a q-range from 0.0019 to 0.64 $Å^{-1}$. All measurements were done under atmospheric pressure and room temperature. Measurements were performed in quartz Hellma cells with an optical path of 1 mm. Standard corrections for sample volume, neutron beam transmission, empty cell signal subtraction and detector efficiency were applied to obtain the scattered intensities. The absolute scale (cm^{-1}) was calculated by normalization with the incident neutron beam. The data reduction has been done using 'PASINET' software. The SANS measurement of the same sample on absolute scale is the most precise method to determine the average composition of an aggregate in a multi-component system [24].

2.9. Self-diffusion NMR experiments

The self-diffusion coefficients were determined at 293K on a Bruker 500 MHz equipped with a broadband inverse (BBI) probehead with z gradient, using the ^{1}H pulsed field gradient stimulated echo technique. The following parameters were used: intergradient delay of 100 ms, gradients of sinusoidal shape and duration of 2 ms, interscan delay of 2.5 ms, 32 scans. Ten points (ten gradient strength values) were recorded per sample, which was enough to determine diffusion coefficient with a few percent precision. Some points were cross-checked via a routine DOSY sequence.

3. Results and discussions

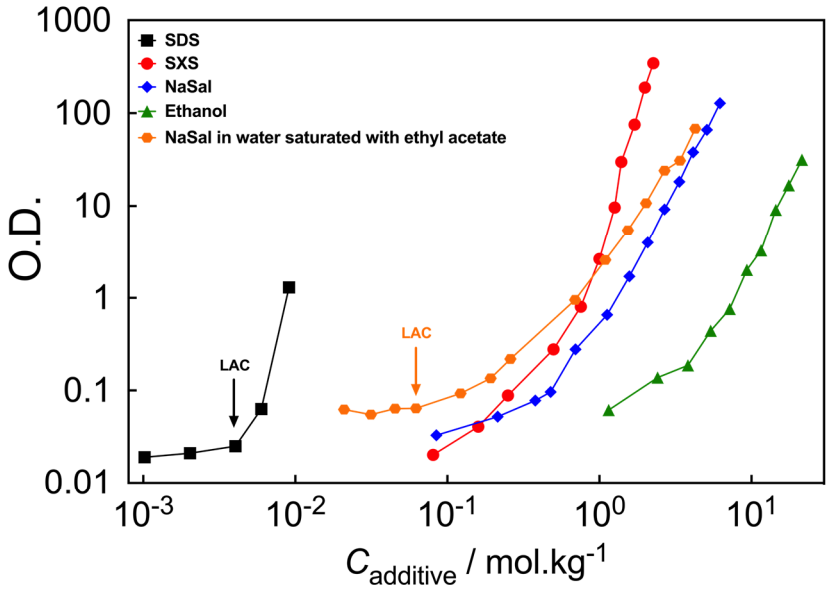

Figure 1: Optical densities, proportional to the amount of the dissolved Disperse Red 13 dye, versus the concentration of SDS (■), SXS (●), Ethanol (▲) and NaSal (◆) in water and the concentration of NaSal in water saturated with EA (●) (4 wt% EA in water) at 25˚C.

3.1. Disperse Red 13 solubilisation in the binary water/surfactant or hydrotrope systems

The easiest method to determine the hydrotropic properties of a molecule is to measure the optical density of a standard hydrophobic dye [3] (see experimental section 2.2.). The measured optical densities as a function of concentration of SDS, SXS, Nasal, Ethanol and NaSal saturated with ethyl acetate are plotted in a logarithmic scale in Figure 1. The logarithmic scale allows one to compare all solubilisation curves over a large range of concentrations. Moreover, the logarithm of the concentrations is directly proportional to the chemical potential. Hydrotropes are efficient in solubilizing the dye, however a factor of hundred increase of concentration is needed for solubilization by a hydrotrope compared to a surfactant. A typical surfactant such as SDS shows a curve featuring a break not at the cmc, but at the lowest aggregation concentration (LAC). The cmc is the concentration at which micelles are dominant over monomers in binary solution. In the presence of a hydrophobic solute, micelles can nucleate around a solute molecule and be present even at a concentration lower than the cmc. The onset of concentration when this happens is called LAC [25–27].

As expected, the solubilisation of DR-13 starts at a lower SDS concentration, compared to the other additives. The most commonly used hydrotrope, ethanol, is one of the least efficient ones (triangle curve on the right). The curve of one of the most common charged hydrotropes (sodium xylene sulfonate, SXS) is located between classical surfactant on the left and weaker hydrotrope such as ethanol on the right. If we compare SXS to NaSal, the curves are very similar: the molecular volume (0.298 nm^3/molecule for SXS and NaSal) are also comparable, but the “hydrophobicity” of NaSal is much higher than the “hydrophobicity” of SXS (log (P) = -3.12 for SXS and log (P) = -1.43 for NaSal). However, if the NaSal/water mixture is saturated with EA, the dye solubility curve is shifted to the left and also exhibits a more pronounced slope discontinuity characteristic of LAC. The two arrows indicate the LAC for SDS in water and NaSal in water saturated with EA. This indicates that the free energy of nucleation of SDS and NaSal around one dye molecule differs by 5 kJ/mol (RT ln(LAC1/LAC2)). This interesting finding made us investigate the microstructure by means of SAXS and SANS scattering along a NaSal-dilution line of water saturated with EA.

3.2. Ternary Phase diagram determination with critical point localisation and density mapping

The ternary phase diagram of water/NaSal/EA at room temperature is shown in Figure 2. The single,

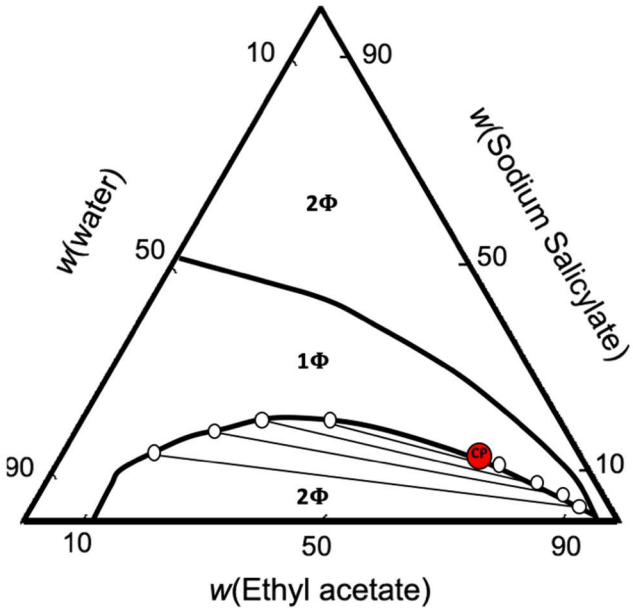

Figure 2: Ternary phase diagram given in weight fractions of water/NaSal/EA including the critical point marked in red at room temperature. Straight black lines indicate the tie-lines obtained from density measurements.

homogenous and thermodynamically stable phase region is located in between two biphasic regions. At low NaSal content, the miscibility gap is closed with a fairly low amount of hydrotrope (around 20%). This is half of the amount of ethanol, which is necessary in the most studied hydrotrope case water/ethanol/octanol [5]. 10 wt% of EA is saturating water, while 4 wt% of water is saturating ethyl acetate. Unlike with most common hydrotropes, the critical point is close to the EA corner (71 wt% EA, 17 wt% NaSal, and 12 wt% water). Another remarkable feature is the asymmetry of the tie-lines. The quantitative differences between classical critical point where only concentrations to heterophase transition a change in local structure has been introduced by Frenkel [28] and detailed in the case of weak aggregation by Shimuzi [29,30].

The second/upper biphasic region corresponds to a liquid-solid equilibrium. Crystals of NaSal precipitate. A small amount of EA probably co-precipitates. No chemical analyses were performed in this multi-phase region, because it was not in the scope of this paper. The maximum solubility of NaSal in water at room temperature is 50 wt%. NaSal is insoluble in ethyl acetate.

To quickly identify the composition of the macroscopically homogeneous fluid near to the separation boundary, an efficient method has been introduced by A. Arce [31]: it requires to prepare a hundred or more samples, for which the density can be easily and precisely measured (see experimental section 2.2.3.). Using the density maps obtained in the monophasic regions, the composition can be indirectly determined with less than 0.1% error in composition. The two-dimensional density map of the ternary mixture studied here is shown in figure 3. Moreover, the density map can be used to identify the regions of interest for structural studies. This requires the conversion of the density into the density excess, which is the difference between the measured density $\rho_{Experimental}$ and the theoretical one $\rho_{theoretical}$. In the absence of non-linear electrostriction effects as well as non-linear effects of solvent cohesion enthalpies in mixtures, the regular solution theory is a good approximation. Regular solution theory expects densities that are extremely close to linear behavior (Equation 1):

$$\rho_{Theoretical} = w_1 \cdot \rho_1 + w_2 \cdot \rho_2 + w_3 \cdot \rho_3 \qquad (1)$$

Where w_i are the weight fractions and ρ_i the densities of pure water, EA and NaSal, respectively.

The ternary contour diagram for density excess is shown in figure 4. Less than 1% of density excess is already the sign of local organization: co-micellization of classical surfactants has been evidenced by pycnometry, nearly a century ago [32].

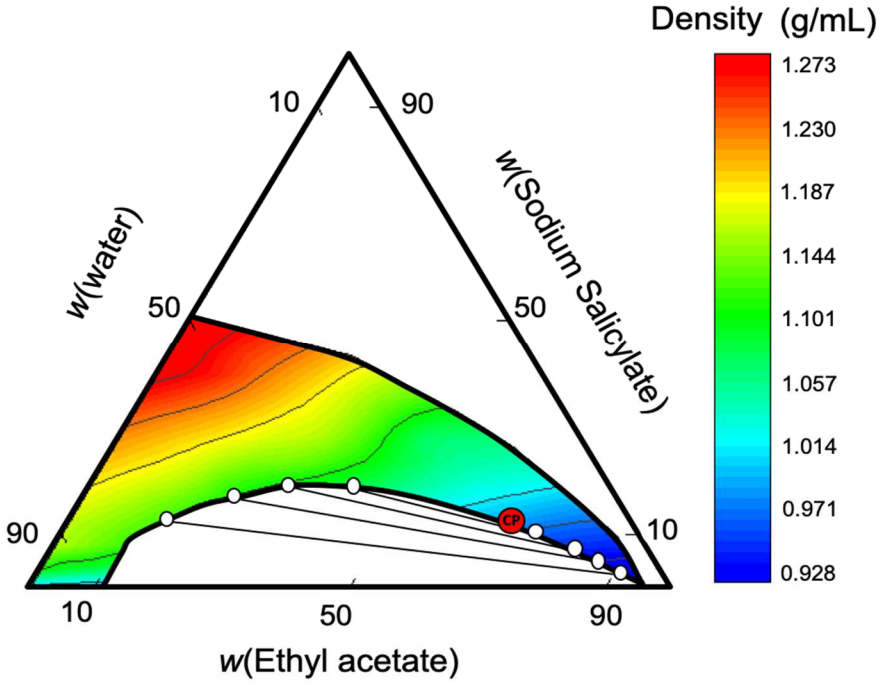

Figure 3: Ternary contour diagram for densities at 25 °C of water/Nasal/EA. Ternary mixtures provided in weight fractions.

The first observation is the absence of detectable density excess around the critical point. This is due to the fact that this critical point is a common critical point without pre-Ouzo like fluctuation. Pre-Ouzo fluctuations in ternary fluids have been evidenced by neutron scattering [24] and have many similarities with pre-transition effects associated to heterophase fluctuations as suggested initially by Frankel [28]. Common critical points with pre-Ouzo like fluctuation have been described for example in the case of water/ethanol/octanol [7,33]. However,

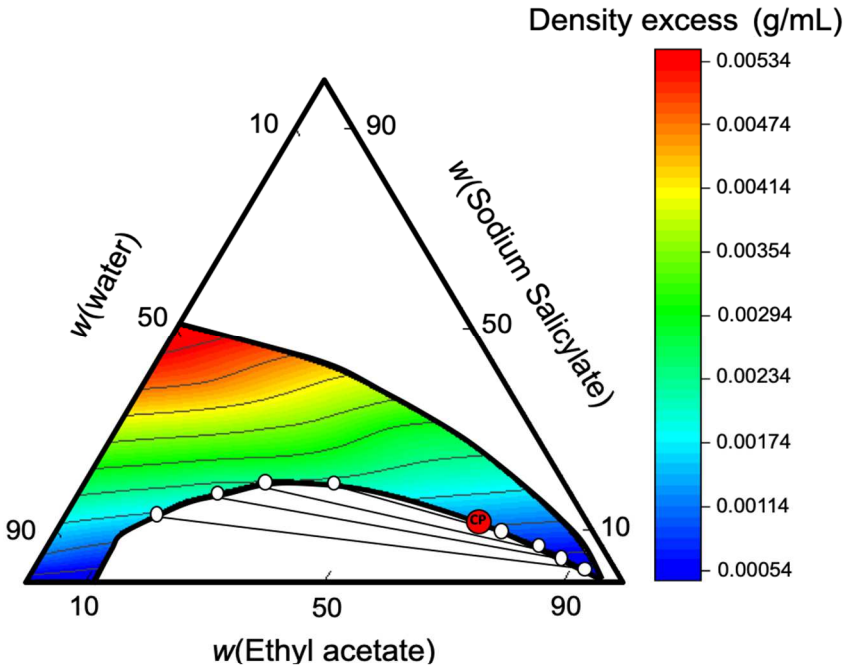

Figure 4: Ternary contour diagram for density excess at 25 °C of water/NaSal/EA. Ternary mixtures provided in weight fractions.

a density excess appears in the EA-poor region, close to the phase boundary and maximum solubilisation of NaSal in water. This is probably an electrostriction effect, due to the first layer of water around the anionic hydrotrope [34,35]. Here again, the situation is different from the water/ethanol/octanol case, for which the density excess is still measurable in the pre-Ouzo region and around the critical point (see supplementary information: figure 6).

3.3. Dynamic light scattering around the critical point.

Dynamic light scattering measurements (Figure 5) around the critical point were performed, because it is the easiest method to check the presence of critical fluctuations (see experimental method 2.2.4.). Common and pre-Ouzo like fluctuation, cannot be discriminated from each other by DLS. Further away from the critical point, no correlated scattering could be detected with DLS, showing the absence of time correlation in the millisecond range. The monomodal correlation times of the DLS in the ternary water/NaSal/EA and water/ethanol/1-octanol are shown in figure 5. In the case of the anionic hydrotrope, the distribution of the correlation times is asymmetric with respect to the water-oil ratio distance from the composition of the critical point and more pronounced on the water-rich side. This is not the case for the reference system with water/ethanol/octanol. In the absence of data related to molecular diffusion, the only information that can be taken from DLS measurement is the presence of a common classical critical point or pre-Ouzo-like fluctuation. Figure 5 shows

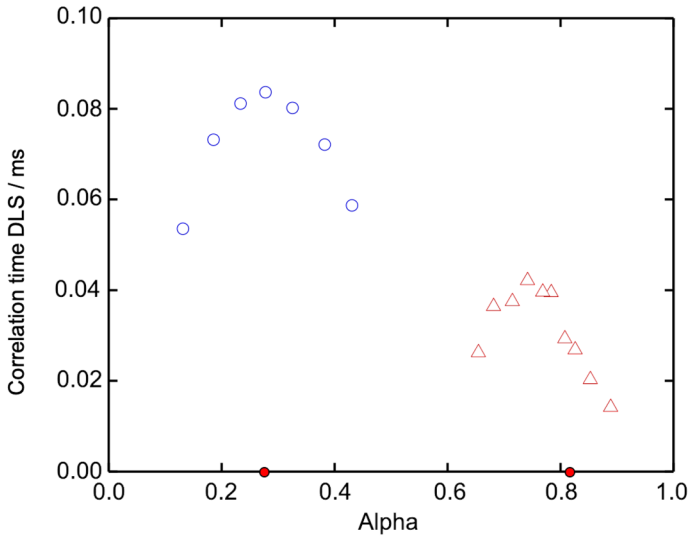

Figure 5: Asymmetry of the distribution of correlation times around the critical point in the case of water/NaSal/EA mixtures (triangular brown icons) compared to the ternary system water/ethanol/1-octanol (circular blue icons). Alpha represents the oil to water ratio in mass fraction. The red dots correspond to the critical points.

both behaviours on the same scale.

3.4. SAXS spectra along dilution lines

The dilution with EA was investigated, starting from a binary water/NaSal mixture. The compositions are shown in the inset of figure 6 (a). The scattering pattern shown in absolute scale with the corresponding colors is plotted on a log-log scale over two decades.

We first consider the compositions near the critical point. Starting from the EA corner, the first four samples investigated are dominated by an Ornstein-Zernike (OZ) behaviour (see supplementary information table 1 and figure 7). All values are less than ten times the molecular length, so they are thermodynamically “far” from the critical point and scaling laws cannot be applied. This OZ-behaviour is consistent with the presence of a common as well as with a pre-Ouzo-like critical point: Near any critical point in ternary fluids, the so-called Ornstein-Zernike (OZ) behaviour, checked by a simple plot of $1/I(q)$ versus q^2, is observed. Deviations from OZ behaviour, when detected are only due to multiple scattering. Detection of large correlation lengths is not the proof of presence of permanent large aggregates, but only a correlation length for “average” size of clusters [36]. Histogram of cluster size is a decaying exponential. Detection of strong OZ-type in scattering is not a

proof neither of the presence nor of the abscence of a preferred transient aggregate size far or near a critical point.

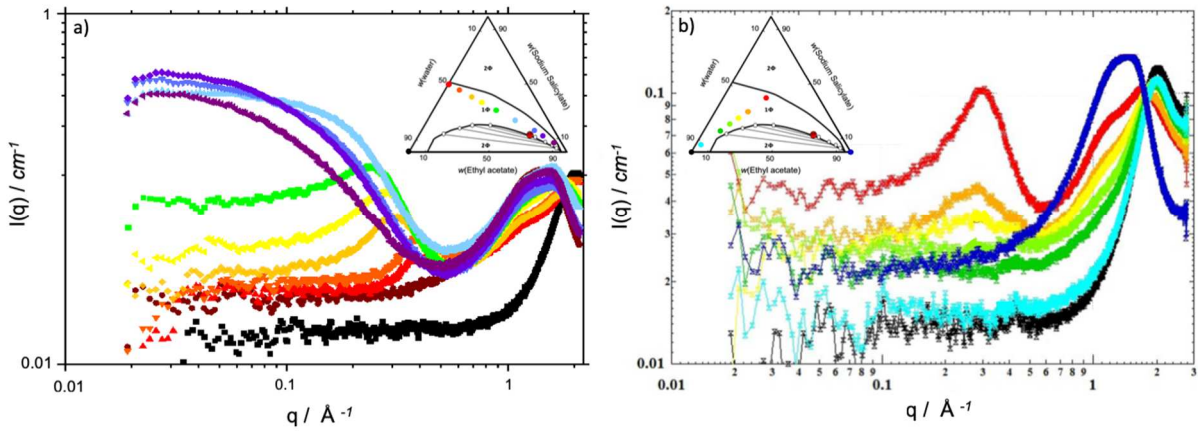

Figure 6: SAXS measurements along dilution lines, as shown on the phase diagrams with (a) increasing amount of oil (EA) (b) increasing amount of water.

Subsequently, we consider the other end of the dilution line, starting from the binary mixture of water and NaSal. The first three investigated points show negligible forward scattering, so there is no pre-peak, in contrast to what is found in most binary solutions of water-miscible molecules [37]. Consequently, there is no self-association of the hydrotrope nor the oil. Therefore, both the binary and the ternary mixtures in this composition range can be considered as regular solutions [38]. In contrast, pre-peaks are present in the range, where excess density anomaly is observed.

The ternary mixtures with the compositions of the yellow and green points show a specific behaviour: forward scattering and a broad peak corresponding to a distance of 2 nm is detected, but without any Porod asymptotic limit. These features are also apparent in the case of weakly aggregating sodium octanoate in water [39] as well as in the ternary system water/sodium octanoate/pentanol [32,40]. The three remarkable features of the scattering curves are:

- Forward scattering I(q=0) is a product of form factor (square of aggregate mass) by osmotic compressibility, when a certain number of aggregates form a pseudo-phase in dynamic equilibrium with non-associated molecules (at the LAC).
- The peak position describes the maximum of the structure factor (S(q)) and corresponds to the most probable distance between aggregates. These aggregates interact via electrostatic repulsion, screened by the monomers present at LAC.
- The Porod limit cannot be measured, since it is hidden by the take-off of the broad liquid band, located at 2 $Å^{-1}$ for water and 1.8 $Å^{-1}$ for hydrocarbons containing mainly CH_2 groups.

The small size of the aggregates hinders the fitting via a three-parameter formula such as the Teubner-Strey one [41]. The most efficient data interpretation can be made by using the decoupling approximation for the calculation of the form factor P(q) and RMSA (Rescaled Mean-Spherical Approximation) for the calculation of the structure factor S(q) [42–44]. This allows the extraction of the average aggregation number as well as of the effective hydrodynamic volume and charge from each peak. Unlike broad peaks analyzed via self-consistent form and structure composition, pre-peaks are usually interpreted via molecular dynamics and explicit calculation of expected small-angle patterns. The repulsive sphere approach RMSA is more adapted, whenever the average number of molecules per aggregates (n) is above ten. The dynamic self-association approach is more adapted in the case of weak aggregation.

The dilution line shown in figure 6 (b) involves dilution by water at constant NaSal to EA ratio. The light blue pattern obtained in the water corner is close to pure water and is typical of a regular ternary solution. The liquid structure peaks are found at 2.1 $Å^{-1}$. At lower water content, the two green patterns show some incoherent (q independent) scattering characteristics of an unstructured ternary fluid. The maximum concentration of NaSal, for which no peaks are visible at q = 0.3 $Å^{-1}$, is 22 wt% of NaSal, i.e. approximately 1 M. Above this NaSal concentration, the same broad peak as observed in the other dilution line is apparent. This is the signature of the

same aggregates including NaSal and EA. A very peculiar feature is that the position of the peak does not move towards high q with increasing NaSal concentration. This means that the average distance between the aggregates does not vary upon concentration of water saturated with EA. This implies that the aggregation number increases quickly with total concentration. In most types of micelles made by conventional surfactants, the aggregation number does not vary when the surfactant concentration is increased from cmc to several times the cmc. This behaviour has been found for example in the case of ionic surfactant SDS. The increase of aggregation number versus concentration close to the cmc is characteristic of short surfactants such as octanoate [39]. In the case of SDS, as in most surfactants, the aggregation number and hence the area per molecule does not vary significantly between cmc and three times the cmc. The slight increase can be understood within the "ladder model" [45]. More precisely, the dehydration of the head-group is the source of the slight increase in aggregation number [46]. In all previously reported cases, the shift to high q of the peak observed for classical micelles is much more pronounced than in the case described here.

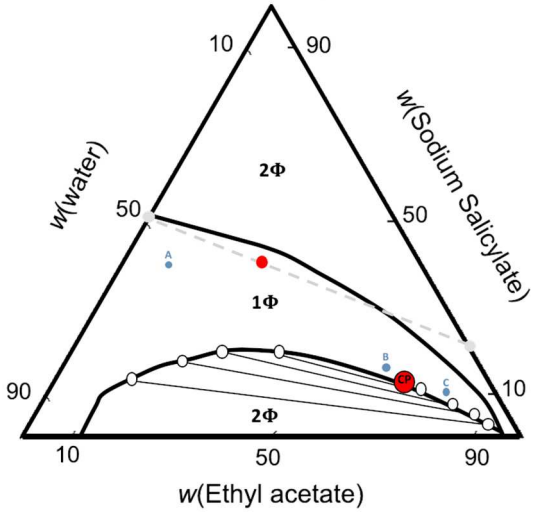

Figure 7: Location of the samples investigated with SAXS and SANS (red icon) and with NMR spin-echo experiments (blue icons). Across the red point, a grey virtual tie-line is drawn.

3.5. SAXS-SANS structural study of the small aggregates

Data fitting was performed using the software 'SASview' and must agree with some physical parameters for SAXS and SANS measurements: this has elucidated the profound difference between weakly aggregated polydisperse micelles and monodisperse aggregates [47]. The expected and calculated patterns are shown with corrections in scale of 1.6 and 7 as multiplied scaling factors, respectively for SANS and SAXS, in Figure 8. In Fig. 7, virtual tie-lines are established like in the former paper with the corresponding water/ethanol/1-octanol system [7]. The scaling factor of SAXS is much more than in commonly accepted range (0.6 to 1.5). This is probably due to the partial molar volume of the sodium salicylate which may well even become negative, thus increasing contrast between aggregate and bulk: the scattering, at least close to vanishing angles, reflects thermodynamics. So it makes sense not to use molar volumes of the pure components, but indeed partial molar volumes. And they can indeed be negative, since the addition of a salt to a certain volume of water can lead to a decrease of the total solution volume compared to the volume of the corresponding pure water.

The virtual binodal line linking two points that correspond to the composition of one NaSal aggregate and the composition of the surrounding solvent has been chosen (see Figure 7) as parallel to the tie-line near the critical point. The dominant fluctuation is the one of ethyl acetate. To validate the choice of the virtual tie-line, self-diffusion constants have been determined by ^{1}H NMR spin-echo experiments, and the results are shown in Table 2.We see that the diffusion coefficient of EA at point A in the phase diagram shown in Fig. 7 is much lower than at points B and C. This means that ethyl acetate diffuses as fully trapped "inside" the aggregates producing scattering at the points, where SAXS and SANS spectra have been recorded.

Table 1: Values of NMR diffusion coefficients for points A, B, and C on the phase diagram, shown in Fig.7 (blue dots) at 500 MHz and

293K.

	Sodium Salicylate ($m^2 \cdot s^{-1}$)	Water ($m^2 \cdot s^{-1}$)	Ethyl Acetate ($m^2 \cdot s^{-1}$)
A	$4.77.10^{-11}$	$2.57.10^{-10}$	$8.40.10^{-11}$
B	$2.18.10^{-10}$	$3.25.10^{-10}$	$1.13.10^{-9}$
C	$2.93.10^{-10}$	$9.12.10^{-10}$	$1.7.10^{-9}$

The resulting parameters for the best fit shown were:

Table 2: Values of calculated SAXS and SANS parameters

parameters	Scale	Background (cm^{-1})	SLD (10^{-6} Å^{-2})	SLD solvent (10^{-6} Å^{-2})	Radius (Å)
SAXS	7	0.001	8.39	8.82	10
SANS	1.6	0.01	0.7	3.3	10

where Scale is the source intensity, SLD is the Layer scattering length density, SLD solvent is Solvent scattering length density and the radius is the sphere radius (see supplementary information for more details about the scattering analysis and formulas of the fitting equations used).

From the dilution line and the general scattering features along it, following questions are open: What is the composition of these aggregates? What is the aggregation number reached before instability to crystallization occurs? What is the balance between steric and electrostatic repulsion between solvent-swollen aggregates?

These three questions can be addressed only via combined X-ray and neutron scattering on an absolute scale [48]

Figure 7 shows the location of the point investigated by SAXS and SANS (the red point) in the phase

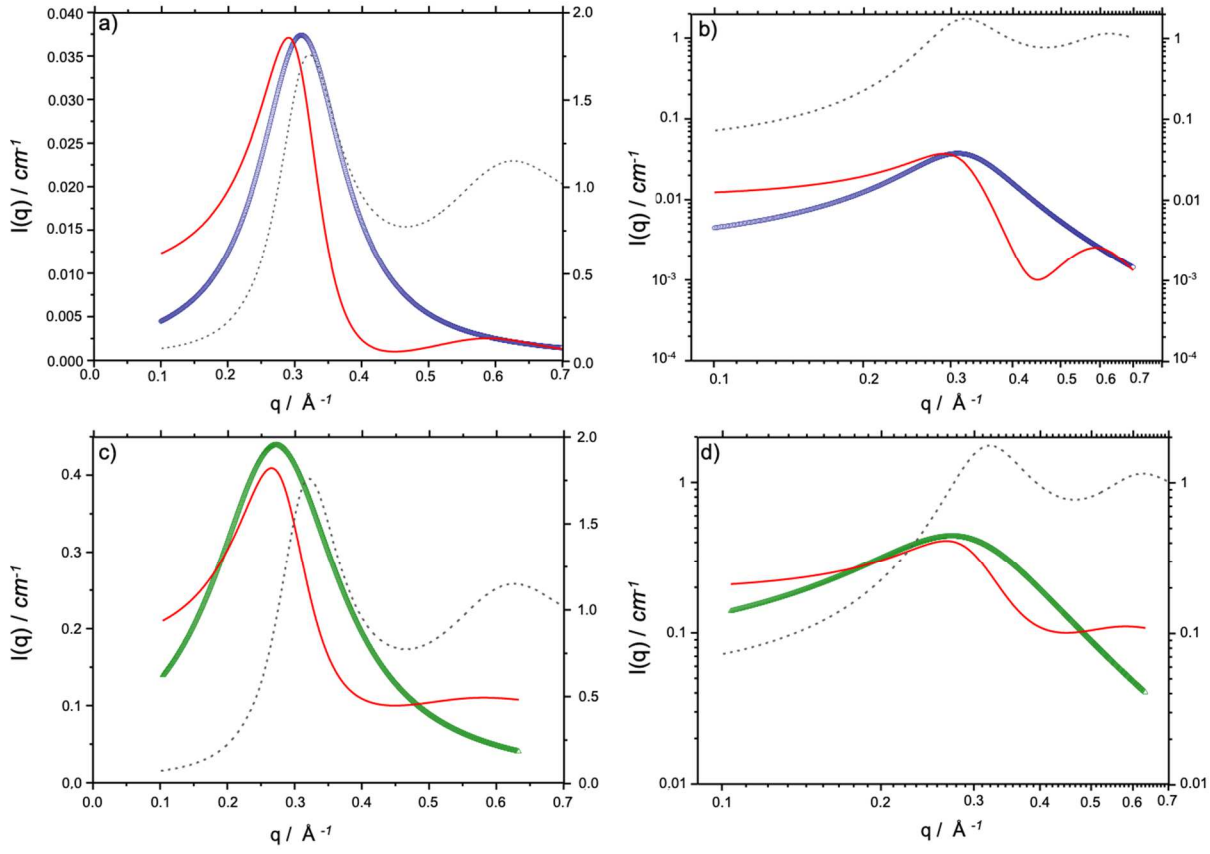

Figure 8: Experimental and simulated Small Angle Scattering curves for the sample with the composition represented in Figure 7. Simulated curves are represented in red, experimental SAXS curves in blue, SANS in green and S(q) in dashed grey line. Left: linear scale; Right: logarithmic scale.

diagram.

Since the point is far from a critical point, the RMSA approximation can be used to evaluate the structure factor S(q). Assuming a virtual tie-line as shown in figure 7 as first approximation, one can generate SAXS and SANS patterns, shown in Figure 8, and compare to experimental ones. A strong constraint is the mandatory common structure factor for SAXS and SANS spectra, as can be seen in figure 8. The dilution experiment along the line shown in the insert of Fig. 6 allows fixing the value of the onset of aggregation to a hydrotrope concentration of 1 M. i.e, half of the NaSal concentration present in the sample considered both with SAXS and SANS.

To catch the main feature of this weak aggregation, the theoretical expectations are calculated with the assumption of monodispersity in the aggregate volume. A relatively sharp scattering peak is measured, but no sign of oscillation at high q. Therefore, conjunction of high-q scattering due to solvent structure in the WAXS region and absence of broadening of the peak suggests a relatively monodisperse aggregate size in the sample. As a first approximation, monodispersity was assumed, as was done in the case of ionic micelles made from conventional surfactant until precisely scaled SANS measurement at high spectral window (q_{min}, q_{max}) in a series of concentration were performed [49]. This simplification induces deviations at high q-values, a fact that cannot be avoided, even when other plots such as a log-normal is considered. So, we accepted this deviation in a first approximation. The main message is that aggregates are made of half a dozen of sodium salicylate and twice this number of EA molecules present in a weak mixed aggregates. these aggregates are water-poor. The counter-ions are not all bound to the surface, so the charge density should be 0.5 charges per nm^2. The electrical repulsion between aggregates is screened, because of the high sodium concentration at the surface of the aggregates. The low q value of the structure factor gives the osmotic compressibility S(0) relative to a perfect gas and is in our case 0.09.

The largest stable aggregate near the crystallization boundary involves 12 NaSal molecules that are swollen aggregates with about the same volume of ethyl acetate, meaning a mole ratio of 1 NaSal to 2 EA inside the aggregates. Outside of the aggregates, the solvent pseudo-phase still contains 1 M of NaSal. It is important to notice that water is not detectable inside the aggregates. However, it should be noted that the self-diffusion coefficient of water decreased slightly, which may be due to the hydration force solvation layer of the emerging aggregates, similar to what was found in the first 1.5 nm near lipid bilayers.

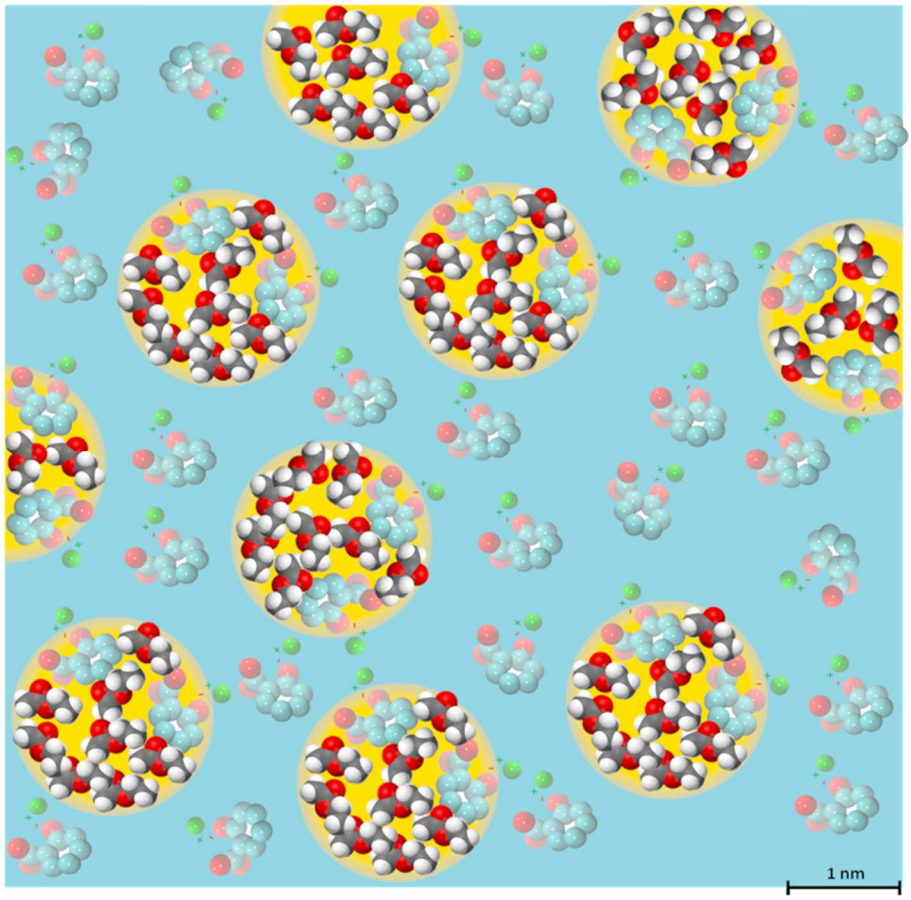

Figure 9: Scaled representation of the structure of the point in the phase diagram investigated with SAXS and SANS. The blue region is the solvent phase whereas the orange one shows the core of the aggregate with 2 NaSal molecules and 8 EA molecules. The distance between aggregates is about 2.5 nm.

Finally, an artist view of the aggregate structure at nm scale with molecules drawn to scale is shown in figure 9. Due to screened electrostatics, the average distance between aggregates is 2.5 nm, similar to their diameter. However, the size of the mixed aggregates and the high value of the minimum aggregation concentration of the hydrotrope is similar to the case of sodium octanoate [39,40]. Neither ethyl acetate as a relatively polar oil nor NaSal as a hydrotrope produce micelles in water alone. The aggregates of sodium salicylate swollen by ethyl acetate could therefore be designed as surfactant-free micelles.

A similar case has been described in another context by Miles Page and co-workers [50]: here, weak pre-nucleation clusters of calcium hydroxide are found, stabilized by preferential adsorption of ethylene glycol over 2-propanol. In this latter case, this preferential adsorption of ethylene glycol in the aggregates is similar to the preferential adsorption of ethyl acetate over water in the case described in the present paper. The aggregates are poor in water, hence all sodium ions must be released. It makes sense that dynamically formed aggregates near the crystallization boundary, as described here, have several features in common such as nm-size, large fractions of un-bound "monomers" and preferential solvation in a two-component solvent, with prenucleation clusters involved in non-classical nucleation [51].

These features are quite general for calcium hydroxide nanoparticles. Typically, those are stabilized in ethylene glycol and propanol mixtures. Also in this case, selective adsorption of ethylene glycol versus 2-propanol was observed [50]. In the sodium salicylate aggregates, preferential adsorption of ethyl acetate versus water is found. The entropic cost of separating water and ethyl acetate limits the growth of the aggregates [52,53] In the literature concerning calcium, the aggregates are designed as nanoparticles, since their size is typically two to ten times larger than NaSal solvent-swollen aggregates described here [53]. In both cases, no Bragg peaks are detected. The particle is an amorphous “nano-phase”.

Another case of adsorbed solvent-stabilized nanoparticles in amorphous state of calcium has been described and investigated by Gebauer and Cölfen [54]: these are named pre-nucleation clusters (PNC). In this case, typically thirty to sixty calcium ions, fifty counter anions, and thirty water molecules formed a PNC [51,54]. In both cases, metastability is observed close to a liquid-solid phase separation boundary. When calcium-based PNCs are diluted, smaller clusters named DOLLOPS are detected [55]. In the present paper, in the first investigation of the effect of dilution with ethyl acetate, this feature could also be detected via the shift to a higher q of the pre-peak.

4. Conclusion and outlooks

In this system based on an electrolytic hydrotrope, we could not find any sign of pre-Ouzo structuring, and we have not encountered spontaneous emulsification, also known as the Ouzo effect. This result is somewhat unexpected, since one could think that the presence of charges may strengthen elusive structures such as the pre-Ouzo aggregates. But the contrary is obviously the case.

Sodium salicylate as the chosen electrolyte hydrotrope is sensitive to the anti-solvent effect of ethyl acetate: thus, there is a new domain of density anomaly that contains lots of DOLLOPS/electrolyte micelles, identified by scattering, with an inter-aggregate distance of 2 nm. Since these aggregates appear close to the hydrated crystal nucleation zone, they can be considered as pre-nucleation clusters in the Gebauer/Kellermeier/Coelfen language. An artist scaled view of the nanostructure at the composition, where pre-nucleation clusters are present, is shown in figure 9. Clearly, here the charged character of the hydrotrope plays a major role.

The third role of hydrotrope charges is visible for EA-saturated aqueous solutions containing more than 1M of NaSal. Here micellar-like structures appear similar to those found in solutions of medium-chain surfactants like sodium octanoate. Such structures have never been found in ternary water-oil-uncharged hydrotrope mixtures with comparable compositions. However, the here found structures are somewhat reminiscent of those that appear when salts, and in particular antagonistic (hydrotropic) salts, are added to the classical water-ethanol-1-octanol system [56]. It seems that, at least in this particular respect, there is some similarity in the structural consequence of either having a charged hydrotrope in the ternary mixture or adding a salt to an oil-water mixture made compatible with an uncharged hydrotrope.

The presented phase diagram of the water/NaSal/EA mixture could be useful for the perfume and pharmaceutical industry, since the chosen hydrotrope is often used in these two industrial sectors. Moreover, ethyl acetate is a major ”green” solvent, commonly used in extraction processes. In following papers, we will show in how far the here described structuring favours extraction and solubilization of natural ingredients.

Acknowledgments

We thankfully acknowledge the CNRS for financial support through the international Research Project “NISI” program. The authors would like to thank Olivier Diat for assistance with SWAXS measurements and for fruitful discussions. We also thank the referees for critical reading and drawing our attention to the complex behaviour of water diffusion.

Appendix A. Supplementary material

The following information is available:
Supplementary data to this article can be found online at

References

[1] W. Kunz, K. Holmberg, T. Zemb, Hydrotropes, Current Opinion in Colloid & Interface Science. 22 (2016) 99–107.
[2] T. Buchecker, S. Krickl, R. Winkler, I. Grillo, P. Bauduin, D. Touraud, A. Pfitzner, W. Kunz, The impact of the structuring of hydrotropes in water on the mesoscale solubilisation of a third hydrophobic component, Phys. Chem. Chem. Phys. 19 (2017) 1806–1816.
[3] P. Bauduin, A. Renoncourt, A. Kopf, D. Touraud, W. Kunz, Unified Concept of Solubilization in Water by Hydrotropes and Cosolvents, Langmuir. 21 (2005) 6769–6775.
[4] S.A. Vitale, J.L. Katz, Liquid Droplet Dispersions Formed by Homogeneous Liquid−Liquid Nucleation: “The Ouzo Effect,” Langmuir. 19 (2003) 4105–4110.
[5] M.L. Klossek, D. Touraud, T. Zemb, W. Kunz, Structure and Solubility in Surfactant-Free Microemulsions, ChemPhysChem. 13 (2012) 4116–4119.
[6] T. Lopian, S. Schöttl, S. Prévost, S. Pellet-Rostaing, D. Horinek, W. Kunz, T. Zemb, Morphologies Observed in Ultraflexible Microemulsions with and without the Presence of a Strong Acid, ACS Central Science. 2 (2016) 467–475.
[7] T.N. Zemb, M. Klossek, T. Lopian, J. Marcus, S. Schöettl, D. Horinek, S.F. Prevost, D. Touraud, O. Diat, S. Marčelja, W. Kunz, How to explain microemulsions formed by solvent mixtures without conventional surfactants, Proceedings of the National Academy of Sciences. 113 (2016) 4260–4265.
[8] A. Shojaii, M. Motaghinejad, S. Norouzi, M. Motevalian, Evaluation of anti-inflammatory and analgesic activity of the extract and fractions of Astragalus hamosus in animal models, Iranian Journal of Pharmaceutical Research. 14 (2015) 263–269.
[9] Y.C. Terrie, A pharmacist’s guide to OTC therapy, Pharmacy Times. 75 (2009) 16–19.
[10] R. Revathi, T. Ethiraj, V.S. Saravanan, V. Ganeshan, V. Saranya, T. Sengottuvel, New spectroscopic determination of nifedipine using hydrotropic solubilization, International Journal of Pharmacy and Pharmaceutical Sciences. 2 (2010) 74–76.
[11] K. Nidhi, S. Indrajeet, M. Khushboo, K. Gauri, D.J. Sen, Hydrotropy: A promising tool for solubility enhancement: A review, International Journal of Drug Development and Research. 3 (2011) 26–33.
[12] R.K. Maheshwari, V. Chavada, S. Varghese, K. Shahoo, Analysis of bulk sample of salicylic acid by application of hydrotropic solubilization method, Indian Journal of

Pharmaceutical Sciences. 70 (2008) 823–825.
[13] R.K. Maheshwari, A novel application of hydrotropic solubilization in the analysis of bulk samples of ketoprofen and salicylic acid, Asian Journal of Chemistry. 18 (2006) 393–396.
[14] S.J. Hersey, R.T. Jackson, Effect of Bile Salts on Nasal Permeability In Vitro, Journal of Pharmaceutical Sciences. 76 (1987) 876–879.
[15] P. Schwenger, E.Y. Skolnik, J. Vilcek, Inhibition of Tumor Necrosis Factor-induced p42/p44 Mitogen-Activated Protein Kinase Activation by Sodium Salicylate, J. Biol. Chem. 271 (1996) 8089–8094.
[16] C. Rae, S. Langa, S.J. Tucker, D.J. MacEwan, Elevated NF- B responses and FLIP levels in leukemic but not normal lymphocytes: reduction by salicylate allows TNF-induced apoptosis, Proceedings of the National Academy of Sciences. 104 (2007) 12790–12795.
[17] R. Elewa, C.C. Zouboulis, Molecular mechanisms of action of topical antiaging compounds, Journal of the Egyptian Women's Dermatologic Society. 11 (2014).
[18] E. Merinville, A.J. Byrne, A.V. Rawlings, A.J. Muggleton, A.C. Laloeuf, Original Contribution: Three clinical studies showing the anti-aging benefits of sodium salicylate in human skin, Journal of Cosmetic Dermatology. 9 (2010) 174–184.
[19] M.-H. Salagoïty-Auguste, A. Bertrand, Wine phenolics—analysis of low molecular weight components by high performance liquid chromatography, Journal of the Science of Food and Agriculture. 35 (1984) 1241–1247.
[20] F. Bonilla, M. Mayen, J. Merida, M. Medina, Extraction of phenolic compounds from red grape marc for use as food lipid antioxidants, Food Chemistry. 66 (1999) 209–215.
[21] K.H. Young, S.L. Bullock, D.M. Melvin, C.L. Spruill, Ethyl acetate as a substitute for diethyl ether in the formalin-ether sedimentation technique., J. Clin. Microbiol. 10 (1979) 852.
[22] C. Breil, M. Abert Vian, T. Zemb, W. Kunz, F. Chemat, "Bligh and Dyer" and Folch Methods for Solid–Liquid–Liquid Extraction of Lipids from Microorganisms. Comprehension of Solvatation Mechanisms and towards Substitution with Alternative Solvents, International Journal of Molecular Sciences. 18 (2017) 708.
[23] M. Clausse, L. Nicolas-Morgantini, A. Zradba and D. Touraud, in Surfactant Science Series (Vol. 24) Microemulsion Systems, eds. H. L. Rosano and M. Clausse, Dekker, New York, 1987, p. 15., in: n.d.
[24] O. Diat, M.L. Klossek, D. Touraud, B. Deme, I. Grillo, W. Kunz, T. Zemb, Octanol-rich and water-rich domains in dynamic equilibrium in the pre-ouzo region of ternary systems containing a hydrotrope, Journal of Applied Crystallography. 46 (2013) 1665–1669.
[25] P. Ekwall, L. Mandell, K. Fontell, Solubilization in Micelles and Mesophases and the Transition from Normal to Reversed Structures, Molecular Crystals. 8 (1969) 157–213.
[26] K. Fontell, L. Mandell, H. Lehtinen, P. Ekwall, The three-component system sodium caprylate-decanol-water : III the structure of the mesophases, Acta Chemica Scandinavica. 74 (1968) 1–56.
[27] L. Mandell, P. Ekwall, The three-component system sodium caprylate-decanol-water : I. the phase equilibria at 20 C, Acta Chemica Scandinavica. 74 (1968) 1–116.
[28] J. Frenkel, A General Theory of Heterophase Fluctuations and Pretransition Phenomena, J. Chem. Phys. 7 (1939) 538–547.
[29] S. Shimizu, N. Matubayasi Unifying hydrotropy under Gibbs phase rule, Phys. Chem. Chem. Phys. 19 (2017) 23597-23605.
[30] S. Shimizu, N. Matubayasi, Statistical thermodynamic foundation for mesoscale aggregation in ternary mixtures, Phys. Chem. Chem. Phys. 20 (2018) 13777–13784.
[31] A. Arce, A. Blanco, A. Soto, I. Vidal, Densities, refractive indices, and excess molar volumes of the ternary systems water + methanol + 1-octanol and water + ethanol + 1-octanol

and their binary mixtures at 298.15 K, J. Chem. Eng. Data. 38 (1993) 336–340.
[32] Y. Chevalier, T. Zemb, The structure of micelles and microemulsions, Reports on Progress in Physics. 53 (1990) 279–371.
[33] S. Shimizu, N. Matubayasi, Hydrotropy and scattering: pre-ouzo as an extended near-spinodal region, Phys. Chem. Chem. Phys. 19 (2017) 26734–26742.
[34] Y. Marcus, Electrostriction in electrolyte solutions, Chem. Rev. 111 (2011) 2761–2783.
[35] Y. Marcus, Ions in Solution and their Solvation, John Wiley & Sons Inc, New York, 2015.
[36] D.W. Oxtoby, W.M. Gelbart, Depolarized light scattering near the gas-liquid critical point, J. Chem. Phys. 60 (1974) 3359–3367.
[37] M. Tomšič, A. Jamnik, G. Fritz-Popovski, O. Glatter, L. Vlček, Structural Properties of Pure Simple Alcohols from Ethanol, Propanol, Butanol, Pentanol, to Hexanol: Comparing Monte Carlo Simulations with Experimental SAXS Data, J. Phys. Chem. B. 111 (2007) 1738–1751.
[38] J.H. Hildebrand, An improvement in the theory of regular solutions, Proc Natl Acad Sci USA. 76 (1979) 6040.
[39] J.B. Hayter, T. Zemb, Concentration-dependent structure of sodium octanoate micelles, Chemical Physics Letters. 93 (1982) 91–94.
[40] B. Hayter, M. Hayoun, T. Zemb, Neutron scattering study of pentanol solubilization in sodium octanoate micelles, Colloid and Polymer Science. 262 (1984) 798–803.
[41] M. Teubner, R. Strey, Origin of the scattering peak in microemulsions, J. Chem. Phys. 87 (1987) 3195–3200.
[42] B. Cabane, R. Duplessix, T. Zemb, High resolution neutron scattering on ionic surfactant micelles : sds in water, J. Phys. France. 46 (1985) 2161–2178.
[43] J.-P. Hansen, J.B. Hayter, A rescaled MSA structure factor for dilute charged colloidal dispersions, Molecular Physics. 46 (1982) 651–656.
[44] J.B. Hayter, J. Penfold, An analytic structure factor for macroion solutions, Molecular Physics. 42 (1981) 109–118.
[45] S.H. Chen, Small Angle Neutron Scattering Studies of the Structure and Interaction in Micellar and Microemulsion Systems, Annu. Rev. Phys. Chem. 37 (1986) 351–399.
[46] B.L. Bales, L. Messina, A. Vidal, M. Peric, O.R. Nascimento, Precision Relative Aggregation Number Determinations of SDS Micelles Using a Spin Probe. A Model of Micelle Surface Hydration, J. Phys. Chem. B. 102 (1998) 10347–10358.
[47] T. Zemb, P. Charpin, Micellar structure from comparison of X-ray and neutron small-angle scattering, J. Phys. France. 46 (1985) 249–256.
[48] T. Zemb, O. Diat, What can we learn from combined SAXS and SANS measurements of the same sample containing surfactants?, Journal of Physics: Conference Series. 247 (2010) 012002.
[49] J.B. Hayter, Quasielastic Neutron Spin-Echo Spectroscopy, in: S.-H. Chen, B. Chu, R. Nossal (Eds.), Scattering Techniques Applied to Supramolecular and Nonequilibrium Systems, Springer US, Boston, MA, 1981: pp. 49–73.
[50] E. Fratini, M.G. Page, R. Giorgi, H. Cölfen, P. Baglioni, B. Demé, T. Zemb, Competitive Surface Adsorption of Solvent Molecules and Compactness of Agglomeration in Calcium Hydroxide Nanoparticles, Langmuir. 23 (2007) 2330–2338.
[51] D. Gebauer, M. Kellermeier, J.D. Gale, L. Bergström, H. Cölfen, Pre-nucleation clusters as solute precursors in crystallisation, Chem. Soc. Rev. 43 (2014) 2348–2371.
[52] A. Ben-Naim, Molecular theory of solutions, Oxford University Press, 2006.
[53] A. Ben-Naim, Molecular Theory of Water and Aqueous Solutions, World Scientific Publishing Company, 2009.

[54] D. Gebauer, A. Völkel, H. Cölfen, Stable Prenucleation Calcium Carbonate Clusters, Science. 322 (2008) 1819.
[55] R. Demichelis, P. Raiteri, J.D. Gale, D. Quigley, D. Gebauer, Stable prenucleation mineral clusters are liquid-like ionic polymers, Nature Communications. 2 (2011) 590.
[56] J. Marcus, D. Touraud, S. Prévost, O. Diat, T. Zemb, W. Kunz, Influence of additives on the structure of surfactant-free microemulsions, Phys. Chem. Chem. Phys. 17 (2015) 32528–32538.